ULTRA-HIGH FREQUENCY SCANNING CAVITIES FOR NON-RELATIVISTIC ELECTRON BEAM

G. Oksuzyan†, E. Gazazyan, A. Margaryan, A. Ter-Poghosyan, YerPhI, Yerevan, Armenia,
M. Ivanyan, CANDLE, Yerevan, Armenia

Abstract

Different scanning schemes based on the RF cavities for non-relativistic electron beam have been examined. Optimisation criteria for various types of cavities have been developed. A complete picture of the beam scanning at a given point of interest is obtained.

INTRODUCTION

The subject of the present paper is the principles of choosing the spatial scanning of low-energy electron beams (1-10keV). The source of such beams is, in particular, the target, bombarded by high-energy (>1GeV) electron beams. Several RF scanning facilities are examined. The resolving capacity, with respect to emitted electrons' energies for different energy levels is evaluated. The super-high (microwave) frequency of the below-discussed scanning facilities matches with the electron beams repetition rate in accelerator. In particular, the beam repetition rate in Yerevan Electron Accelerator is equal to $f_0 = \omega_0/2\pi = 2.7973GHz$.

CYLINDRICAL CAVITY

The cylindrical cavity is proposed as one of possible spatial scanning facilities (Fig.1). This cavity is excited by two identical mutually orthogonal and 90° phase-

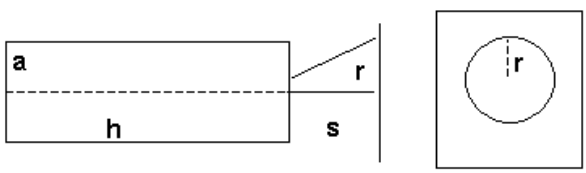

Figure 1. Spatial scanning with cylindrical cavity.

shifted TM_{110} modes [1]. The existing field components of this mode in cylindrical coordinates r,ϕ,z may be presented as:

$$E_z = E_0 J_1(k_c r)\sin\phi\cos\omega_0 t,$$
$$H_\phi = E_0\eta^{-1}J_1'(k_c r)\sin\phi\sin\omega_0 t, \quad (1)$$
$$H_r = -E_0\eta^{-1}J_1(k_c r)/(k_c r)\cos\phi\sin\omega_0 t,$$

with radial propagation constant $k_c = \omega_0/c$. Here $\eta = 120\pi\ \Omega$ is the free space impedance. Orthogonal and 90° phase-shifted mode, realized by replacing $\phi \to \phi + \pi/2$ and $\omega_0 t \to \omega_0 t + \pi/2$, is:

$$E_z = -E_0 J_1(k_c r)\cos\phi\sin\omega_0 t$$
$$H_\phi = E_0\eta^{-1}J_1'(k_c r)\cos\phi\cos\omega_0 t \quad (2)$$
$$H_r = E_0\eta^{-1}J_0(k_c r)/(k_c r)\sin\phi\cos\omega_0 t$$

The total field takes the form:

$$E_z = E_0 J_1(k_c r)\sin(\phi - \omega_0 t),$$
$$H_\phi = \frac{E_0}{\eta}\left(-J_2(k_c r) + \frac{J_1(k_c r)}{k_c r}\right)\cos(\phi - \omega_0 t),$$
$$H_r = \frac{E_0}{\eta}\frac{J_1(k_c r)}{k_c r}\sin(\phi - \omega_0 t) \quad (3)$$

in the cylindrical frame of reference and

$$E_z = E_z \quad (4)$$
$$H_x = -\frac{E_0}{\eta}\frac{J_1(k_c r)}{k_c r}\sin(\omega_0 t) + \frac{E_0}{\eta}J_2(k_c r)\cos(\phi - \omega_0 t)\sin\phi$$
$$H_y = \frac{E_0}{\eta}\frac{J_1(k_c r)}{k_c r}\cos(\omega_0 t) - \frac{E_0}{\eta}J_2(k_c r)\cos(\phi - \omega_0 t)\cos\phi$$

in the Cartesian one. The polarization ellipse equation is:

$$H_x^2\frac{A^2 - L\cos^2\phi}{A^2(A-B)^2} + H_y^2\frac{A^2 - BL\sin^2\phi}{A^2(A-B)^2} - 2H_x H_y\frac{BL\cos\phi\sin\phi}{A^2(A-B)^2} = 1$$

where

$$A = E_0\eta^{-1}J_1(k_c r)/(k_c r),\ B = E_0\eta^{-1}J_2(k_c r),\ L = B(2A - B). \quad (5)$$

The axes of the ellipse are oriented along and perpendicularly to the direction of angle ϕ. In the local coordinate system, connected with this direction, the ellipse equation gets a canonical form:

$$H_x'^2/A^2 + H_y'^2/(A-B)^2 = 1. \quad (6)$$

Semi-axes of polarization ellipse equal to A and $|A-B|$ correspondingly. The radius of the cylindrical cavity is determined from the condition $a = 3.8317/k_c$. For the above-mentioned frequency: $a = 6.54cm$. The height of cylinder should be taken less than half wavelength $\lambda_0 = 10.7246cm$ to avoid higher modes generation. The half axes of the polarization ellipse for the selected cylinder sizes are presented in Fig.2.

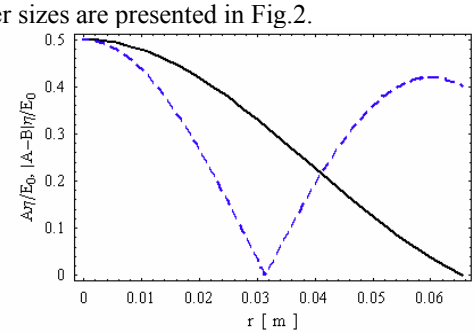

Figure 2. Polarization ellipse half axes for the combined mode TM_{110}. Solid curve: A, dashed: |A-B|.

†oksuzyan@moon.yerphi.am

The equation of the particle motion in the cavity excited by this mode may be written as a differential equations system:

$$\frac{d}{dt}(\gamma m_0 v_x) = -e\mu H_y v_z,$$
$$\frac{d}{dt}(\gamma m_0 v_y) = e\mu H_x v_z, \qquad (7)$$
$$\frac{d}{dt}(\gamma m_0 v_z) = e\left(E_z + v_x \mu H_y - v_y \mu H_x\right),$$

where $\gamma = \left(1 - \left(v_x^2 + v_y^2 + v_z^2\right)/c^2\right)^{-1/2}$ is the Lorenz factor, e is the electron charge and μ is the magnetic permeability of free space. In the common case the initial conditions applied at the moment $t = 0$ of particle entering into cavity with initial coordinates and initial velocities are: $z = 0$, $x = x_0$, $y = y_0$; $v_z = v_{z0}$, $v_x = v_{x0}$, $v_y = v_{y0}$. For the total field one can write down the following using paraxial approaching $(k_c r << 1)$:

$$E_z = 0,\ H_x = -\frac{E_0}{2\eta}\sin\omega_0 t,\ H_y = \frac{E_0}{2\eta}\cos\omega_0 t \qquad (8)$$

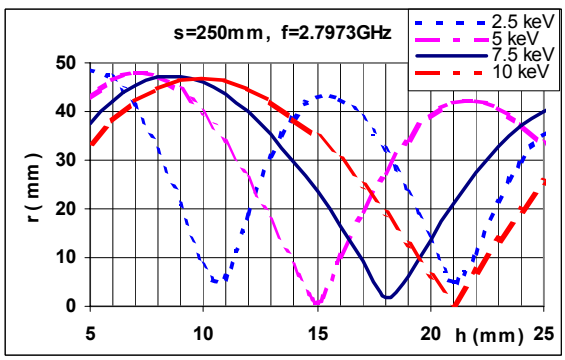

Figure 3. Circle radius distribution versus height of cavity in energy region 2.5-10keV.

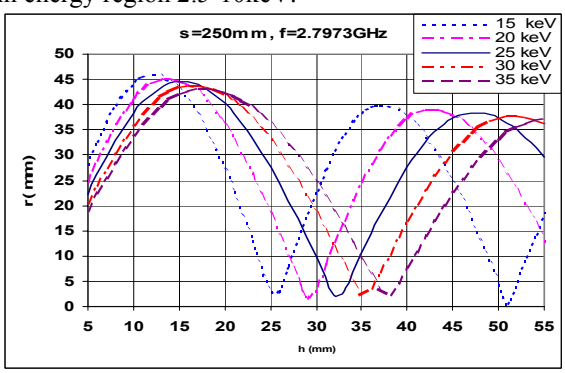

Figure 4. Circle radius distribution versus height of cavity in energy region 15-35keV.

which has a circular polarization, hence the particle displacement plane has a circular rotation in time, and this provides the circular spatial scanning for the bunch particles. The trajectory of the particle, entering the cavity perpendicularly to its cylindrical side has a form of spiral in the cavity and gets a linear shape outside it. In the case of multi-bunch regime the circle-like picture appears on the screen, placed in front of the cavity and parallel to the exit side of it. In Figures 3 and 4 the radii of the circles for the different electron energies, appearing on the screen, are represented.

As it follows from Fig.3, for the cavity height less than 5mm and for the energy region 2.5-10keV we observe an increase in the rings radii when the electron energy decreases. Here a resolution of about 2.1mm/keV may be achieved. Nevertheless, for more narrow energy regions 5-10keV it is possible to obtain an increasing dependence of rings radii on electron energies for higher heights of the cavity (h=11-12mm, Fig.3) with a resolution of ~3.4mm/keV. For higher energy regions (15-35keV, Fig.4) the height of the cavity may be increased up to 10mm to obtain radii increasing with the energy decreasing on the screen with a resolution up to ~ 0.5mm/keV. An increase in energy rings radii for the same energy region may be achieved at h=25mm at an average resolution of ~1.4mm/keV.

RECTANGULAR CAVITIES

In this section the problem of the bunch transition through the rectangular cavities is discussed. For the investigation of the processes of bunch passage through the cavities, FORTRAN-77 computer code has been created. This program calculates optimal cross sizes of cavities to obtain maximal deflecting TE_{102} mode of the field. The working wavelength λ and height h of the cavity are predetermined [2]. The program examines two cases: the bunch transition along the central axis of a single cavity and bunch's sequential passage through two cavities. In the first case a linear shift (A-shift) of the bunch takes place: different particles of the bunch are deflected in different directions in the horizontal plane with a possible imposition on the luminescent screen. The screen is placed at some distance from the back wall of the cavity. In this case the program permits one to obtain the time-shift of the spatial structure of the bunch after its interaction with the deflecting field in the cavity. In the second case the bunch consecutively passes through both of the orthogonal placed identical cavities (Fig.5).

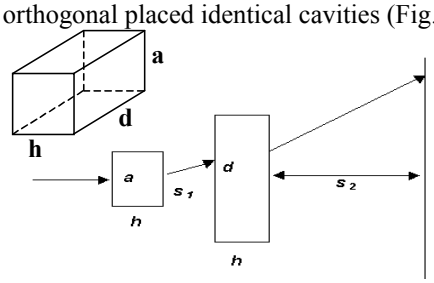

Figure 5. Spatial scanning with rectangular cavities.

In the case of two cavities placed as it is shown in Fig.5, the picture on the screen has the form of an arc of ellipse whose angular length is proportional to the bunch's duration. In the case of tightly placed cavities (s_1=0) the form of the arc on the screen is close to the circle arc.

The program permits one to vary the following parameters: the distance between the cavities (s_1), the distance between the screen and the wall of the second cavity (s_2), the height of the cavity (h), wavelength of

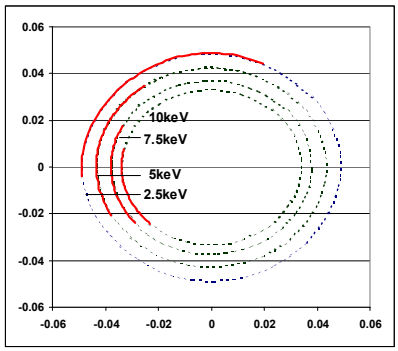

Figure 6. Circular sweep for the bunch energies 2.5-10keV, $s_1 = 0$, $s_2 = 0.25m$, $\Delta\varphi = \pi/2$, $h = 0.5cm$.

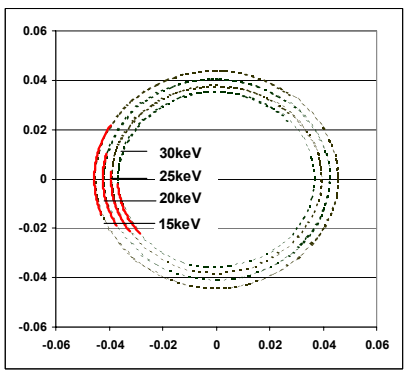

Figure 7. Circular sweep for the bunch energies 15-30keV. $s_1 = 0$, $s_2 = 0.25m$, $\Delta\varphi = \pi/2$, $h = 1cm$.

TEM_{102} mode, the bunch length, the phases shift between the cavities and the bunch energy. The height of cavity is $h \le \lambda/2$, as before. The circular sweeps for bunches with comparatively low (2.5-10keV, Fig.6) and with higher (15-30keV, Fig.7) energies are given. The RMS error, which determines obtained curves deviation from the circular arc, is about 0.15%. The solid curves present the scanned profile of the bunch (single-bunch regime). The bunch duration is equal to $\tau = \alpha T/2\pi$, where: α the angular arc size, T - RF-field period. The images of bunches with different energies have the same length $\lambda/5$ on the screen (Fig. 6,7). The time-duration of a 10keV bunch (Fig.6) is about 60ps.

SLIT-APERTURE RESONATOR

Slit-aperture resonator [3] may be used instead of the rectangular ones in the scheme in Fig.5. The structure of such a resonator consists of the pair of identical circular cylindrical cavities, bounded by a plain cross connection (Fig.8, right) and confined by the cylindrical concavities from both sides (Fig.8, left). This resonator was constructed and manufactured in YerPhI by Oksuzyan G.G. The main sizes of the resonator are:
The distance between the plane plates: $d=2.3mm$
The length (along the x axis) of the plane plate: $l=22mm$
The width of the plates and height of cylinders: $h=8mm$
The radii of the small cylinders: $r_1=r_2=7.5mm$
The radii of the large cylinders: $R_1=R_2=29mm$
The height of the large cylinder: $H=3.5mm$

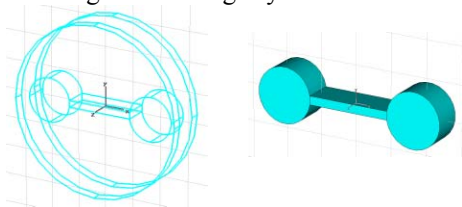

Figure 8. Slit-aperture (left) resonator and uniform bicylindrical (right) cavity.

The eigenfrequencies of the fundamental and several next modes, calculated by Microwave Studio 5.0 software package are presented in Tab.1. The eigenfrequencies of the uniform bicylindrical cavity with the same sizes are given for comparison.

Table 1: The eigenfrequencies of slit-aperture resonator and uniform bicylindrical cavity

	Frequency (GHz)	
N	Quasistat. cavity	Bicyl. cavity
1	2.7876	15.2364
2	3.8756	15.2364
3	3.9100	18.7613
4	5.9597	18.6484

As it follows from the Table, the eigenfrequency of the fundamental mode of the resonator is close to required one. The frequency tuning is included in the structure.

CONCLUSION

The presented spatial scanning schemes may be used for different experimental purposes. Their choice may be made based on the specific conditions of the experiment. The cylindrical cavity, discussed at the top of paper, has a simple structure and consists of a single scanning element. The field's transverse electric component of the fundamental mode of the slit-aperture resonator is strongly uniform in the area between the plates.

This work is supported by ISTC Project A-372.

REFERENCES

[1] V. Guidi et al, "Sub-PS-Resolution Streak Camera Based on RF-Cavity Deflection," http://psj.nsu.ru/facult/inp/str_cam/about.htm
[2] J. Haimson. "Optimization Criteria for Standing Wave Transverse Magnetic Deflection Cavities," J. Appl. Phys, 1983, pp. 303-331.
[3] M.M. Butslov, S.D. Fanchenko, R.V. Chikin, PTE, 5, 1973, pp. 202-206 (in Russian).